



# Ly $\alpha$ Halos around [O III]-selected Galaxies in HETDEX

Maja Lujan Niemeyer<sup>1</sup> , William P. Bowman<sup>2,3</sup> , Robin Ciardullo<sup>2,3</sup> , Max Gronke<sup>1</sup> , Eiichiro Komatsu<sup>1,4</sup> , Maximilian Fabricius<sup>5,6</sup> , Daniel J. Farrow<sup>5,6</sup> , Steven L. Finkelstein<sup>7</sup> , Karl Gebhardt<sup>7</sup> , Caryl Gronwall<sup>2,3</sup> , Gary J. Hill<sup>7,8</sup> , Chenxu Liu<sup>7</sup> , Erin Mentuch Cooper<sup>7,8</sup> , Donald P. Schneider<sup>2,3</sup> , Sarah Tuttle<sup>9</sup> , and Gregory R. Zeimann<sup>10</sup>

<sup>1</sup> Max-Planck-Institut für Astrophysik, Karl-Schwarzschild-Str. 1, D-85741 Garching, Germany; [maja@mpa-garching.mpg.de](mailto:maja@mpa-garching.mpg.de)

<sup>2</sup> Department of Astronomy & Astrophysics, The Pennsylvania State University, University Park, PA 16802, USA

<sup>3</sup> Institute for Gravitation and the Cosmos, The Pennsylvania State University, University Park, PA 16802, USA

<sup>4</sup> Kavli Institute for the Physics and Mathematics of the Universe (Kavli IPMU, WPI), University of Tokyo, Chiba 277-8582, Japan

<sup>5</sup> Max-Planck-Institut für Extraterrestrische Physik, Gießenbachstraße 1, D-85748 Garching, Germany

<sup>6</sup> Universitäts-Sternwarte München, Scheinerstraße 1, D-81679 München, Germany

<sup>7</sup> Department of Astronomy, The University of Texas at Austin, 2515 Speedway Boulevard, Austin, TX 78712, USA

<sup>8</sup> McDonald Observatory, The University of Texas at Austin, 2515 Speedway Boulevard, Austin, TX 78712, USA

<sup>9</sup> Department of Astronomy, University of Washington, Seattle, WA 98195-1580, USA

<sup>10</sup> Hobby–Eberly Telescope, University of Texas, Austin, TX, 78712, USA

Received 2022 April 27; revised 2022 July 16; accepted 2022 July 20; published 2022 August 1

## Abstract

We present extended Ly $\alpha$  emission out to 800 kpc of 1034 [O III]-selected galaxies at redshifts  $1.9 < z < 2.35$  using the Hobby–Eberly Telescope Dark Energy Experiment. The locations and redshifts of the galaxies are taken from the 3D-HST survey. The median-stacked surface brightness profile of the Ly $\alpha$  emission of the [O III]-selected galaxies agrees well with that of 968 bright Ly $\alpha$ -emitting galaxies (LAEs) at  $r > 40$  kpc from the galaxy centers. The surface brightness in the inner parts ( $r < 10$  kpc) around the [O III]-selected galaxies, however, is 10 times fainter than that of the LAEs. Our results are consistent with the notion that photons dominating the outer regions of the Ly $\alpha$  halos are not produced in the central galaxies but originate outside of them.

*Unified Astronomy Thesaurus concepts:* [High-redshift galaxies \(734\)](#); [Circumgalactic medium \(1879\)](#); [Intergalactic medium \(813\)](#); [Galaxy environments \(2029\)](#)

## 1. Introduction

Extended Ly $\alpha$  emission around star-forming galaxies without an active galactic nucleus (AGN) has been found around Lyman-break galaxies (LBGs; e.g., Steidel et al. 2011; Kusakabe et al. 2022) and LAEs (e.g., Wisotzki et al. 2016; Kikuchihara et al. 2022; Ouchi 2019, for a review on LAEs). One source of Ly $\alpha$  photons is the local recombination of hydrogen atoms ionized by photons from young, massive stars in star-forming regions. After their escape from the interstellar medium (ISM), Ly $\alpha$  photons will be scattered by neutral hydrogen atoms in the circumgalactic medium (CGM) and intergalactic medium (IGM). Hydrogen atoms in the CGM and IGM can also be ionized by photons from more distant AGNs or star-forming regions, called the ultraviolet (UV) background, and recombine to emit Ly $\alpha$  photons (“fluorescence”; e.g., Gould & Weinberg 1996). Ly $\alpha$  photons from satellite galaxies (Mas-Ribas et al. 2017) and collisional excitation of hydrogen atoms in cooling gas (“cooling radiation”; e.g., Haiman et al. 2000) can add to the extended Ly $\alpha$  emission.

Because the contribution of scattered photons from the central galaxy to the halo depends on the galaxy’s Ly $\alpha$  emission, comparing the Ly $\alpha$  surface brightness (SB) profiles of galaxies with different intrinsic Ly $\alpha$  luminosities or escape fractions can probe the origin of Ly $\alpha$  halos. Because LAEs are selected using their large Ly $\alpha$  equivalent width (EW), they

comprise a biased subset of high-redshift galaxies that have a large Ly $\alpha$  escape fraction along the line of sight (LOS). Galaxies selected via other methods such as LBGs or via their rest-frame optical emission lines may have similar physical properties, but with smaller Ly $\alpha$  escape fractions than LAEs. Erb et al. (2016), Hathi et al. (2016), Trainor et al. (2016, 2019), and Reddy et al. (2022) argue that LAEs have different properties from other star-forming galaxies, such as less dust and metal content, lower star formation rates (SFR) and stellar masses, and higher H I covering fractions. Conversely, Hagen et al. (2016) and Shimakawa et al. (2017) report no statistical difference between the properties of the samples of LAEs and rest-frame optical emission-line galaxies except at high stellar masses. Hence, comparing the Ly $\alpha$  halo profiles of LAEs with those of rest-frame-optical emission-line galaxies can shed light on the emission sources and mechanisms of Ly $\alpha$  halos.

We compare the median-stacked Ly $\alpha$  SB profile of 1034 galaxies at  $1.9 < z < 2.35$  selected via their rest-frame optical emission lines in the 3D-HST survey (Brammer et al. 2012; Momcheva et al. 2016; Bowman et al. 2019, 2020) with that of LAEs at  $1.9 < z < 3.5$  detected in the Hobby–Eberly Telescope Dark Energy Experiment (HETDEX; Gebhardt et al. 2021; Hill et al. 2021; Lujan Niemeyer et al. 2022, hereafter LN22). We use integral-field spectroscopic data from HETDEX to extract the Ly $\alpha$  SB profiles.

We adopt a flat  $\Lambda$  cold-dark-matter cosmology with  $H_0 = 67.37 \text{ km s}^{-1} \text{ Mpc}^{-1}$  and  $\Omega_{m,0} = 0.3147$  (Planck Collaboration et al. 2020). All distances are in units of physical kiloparsecs (kpc) unless noted otherwise.



Original content from this work may be used under the terms of the [Creative Commons Attribution 4.0 licence](#). Any further distribution of this work must maintain attribution to the author(s) and the title of the work, journal citation and DOI.

## 2. Data and Galaxy Samples

### 2.1. HETDEX Data

We use spectra from the HETDEX survey (Gebhardt et al. 2021), specifically internal data release 3. The survey uses the VIRUS instrument on the 10 m Hobby–Eberly Telescope (HET). See Hill et al. (2021) for details.

VIRUS consists of up to 78 integral-field unit fiber arrays (IFUs), each of which contains 448  $1''.5$  diameter fibers and covers  $51'' \times 51''$  on the sky. The fibers from each IFU are fed to a low-resolution ( $R \simeq 800$ ) spectrograph covering 3500–5500 Å. The IFUs with  $\simeq 35$  k total fibers are distributed on a grid with  $100''$  spacing throughout the  $18'$  diameter of the telescope’s field of view. Each HETDEX observation comprises three 6 minute exposures, which are dithered to fill in gaps between the fibers. Because the gaps between the IFUs remain in an individual observation, the filling factor is  $\simeq 1/4.6$ .

We use the full-frame sky-subtracted data (details in Gebhardt et al. (2021), LN22). This sky-subtraction method measures the sky emission from the entire  $18'$  diameter field of view of VIRUS to ensure that extended emission on the scale of an IFU or larger is not removed along with the sky model. The full-frame sky subtraction in the internal HETDEX DR 3 has some differences from that in DR 2, which is used in LN22. Instead of roughly 75% of the total fibers with the lowest continuum emission, only 50% are used for the sky estimate. This helps prevent the oversubtraction of continuum emission due to unresolved sources. To be more conservative, the smooth background subtraction within a six fibers by 600 Å window is omitted. These changes do not affect our measurement because we perform a local continuum subtraction. As expected, the  $\text{Ly}\alpha$  SB profiles of the LAEs using the data from DR 3 and DR 2 and the same stacking procedure are very similar. We mask the wavelength regions around the brightest sky emission lines to avoid residuals associated with this component.

### 2.2. [O III]-galaxy Sample

Our [O III]-galaxy sample is drawn from 3D-HST (Brammer et al. 2012; Momcheva et al. 2016), an HST Treasury program that used two-orbit exposures with the WFC3 G141 grism to observe  $\simeq 625$  arcmin<sup>2</sup> of sky within the Cosmic Assembly Near-IR Deep Extragalactic Legacy Survey (CANDELS; Grogin et al. 2011; Koekemoer et al. 2011) footprint. Bowman et al. (2019) vetted this data set to define a sample of  $\simeq 2000$  optical emission-line galaxies with IR continuum magnitude  $m_{\text{J+JH+H}} < 26$ , unambiguous emission-line redshifts between  $1.90 < z < 2.35$ , and a 50% line-flux completeness limit of  $\sim 4 \times 10^{-17}$  erg cm<sup>-2</sup> s<sup>-1</sup>. In over 90% of the sample, the brightest emission line in the spectral region surveyed by the grating is [O III]  $\lambda 5007$ ; in 90% of the remaining galaxies, [O II] dominates. Most AGNs have been removed from this data set via comparisons with X-ray source catalogs, and Bowman et al. (2019) estimate the fraction of remaining AGN to be less than 5%.

More than half of the Bowman et al. (2019) sample has been surveyed as part of the science verification for the HETDEX survey (Gebhardt et al. 2021); this data set includes over 900 galaxies that have been observed more than once, with some being observed up to 15 times. These repeat observations partly cover the gaps between IFUs and provide a better spatial sampling of the datacube. Weiss et al. (2021) measured the

mean  $\text{Ly}\alpha$  escape fraction of the subsample of these galaxies present in HETDEX DR2 ( $6_{-0.5}^{+0.6}\%$ ) and determined the systematic behavior of the  $\text{Ly}\alpha$  escape versus stellar mass, SFR, internal extinction, half-light radius, and excitation.

We only include HETDEX observations with good seeing (point-spread function (PSF) FWHM  $< 1''.7$ ) and observing conditions (total system throughput  $> 0.1 = 13$ th percentile). These requirements are less strict than for the LAE sample because too few observations of [O III] galaxies meet these requirements. We inspect the remaining observations and exclude data with obvious artifacts such as interference patterns. We require that for an [O III] galaxy’s halo to be included in our analysis, the center of the galaxy must lie within  $3''$  of the center of a HETDEX fiber. A total of 1034 [O III] galaxies (in 44 HETDEX observations) meet our selection criteria, with 57 ( $\simeq 6\%$ ) having a  $\text{Ly}\alpha$  detection in HETDEX (within  $3''$  and  $15$  Å of the expected emission line). Each galaxy was observed in 1–15 separate observations; thus, there are 7401 individual observations of the 1034 galaxies. Their mean redshift is  $\langle z \rangle = 2.1$ .

Because of the abundance of imaging data in the CANDELS fields, the physical properties of our [O III] sample have been well characterized, with stellar masses between  $8.2 \lesssim \log_{10} M/M_{\odot} \lesssim 11.4$  (median mass of  $\log_{10} M/M_{\odot} = 9.3$ ), SFRs between  $0.02 \lesssim \text{SFR} \lesssim 250 M_{\odot} \text{ yr}^{-1}$  (median value of  $1.9 M_{\odot} \text{ yr}^{-1}$ ), internal extinctions between  $0 \lesssim E(B-V) \lesssim 0.6$  (median of  $E(B-V) = 0.09$ ), and optical half-light radii  $R_e \lesssim 5$  kpc (with a median of 1.4 kpc). The full distribution of these properties, along with their [O III] luminosity function and equivalent width distribution, can be found in Bowman et al. (2019, 2020, 2021).

To study the potential dependence of the  $\text{Ly}\alpha$  SB profile on various galaxy properties, we form two subsamples above and below the median observed  $L_{[\text{O III}]}$  ( $41.3 \lesssim \log_{10} L \text{ erg}^{-1} \text{ s} \lesssim 43.1$ , median 42.1, 517/517 sources above/below), SFR (517/517 sources above/below), stellar mass (517/517 sources above/below),  $\text{H}\beta$  flux ( $\lesssim 8 \times 10^{-17}$  erg s<sup>-1</sup> cm<sup>-2</sup>, median  $10^{-17}$  erg s<sup>-1</sup> cm<sup>-2</sup>, 516/518 sources above/below), [O II] flux ( $\lesssim 1.7 \times 10^{-16}$  erg s<sup>-1</sup> cm<sup>-2</sup>, median  $2 \times 10^{-17}$  erg s<sup>-1</sup> cm<sup>-2</sup>, 517/517 sources above/below), dust attenuation (515/519 sources above/below), and UV luminosity ( $25.4 \lesssim \log_{10} L_{1600} \text{ erg}^{-1} \text{ s Hz} \lesssim 29.4$ , median 28.5, 517/517 sources above/below). We also fit a line to the SFR as a function of stellar mass and create subsamples above and below this linear relation (459/575 sources above/below). We omitted unrealistic values from the spectral-energy-distribution fits in the property ranges above.

We estimate the virial radius of the host dark matter halos using the stellar mass–halo mass relation of Behroozi et al. (2019). Roughly 68% of the galaxies in our [O III] sample have stellar masses between  $10^{8.8}$  and  $10^{9.9} M_{\odot}$  and therefore reside in  $10^{11.4}$  to  $10^{11.9} M_{\odot}$  dark matter halos. Following the definition of  $r_{\text{vir}}$  of Bryan & Norman (1998), we obtain  $r_{\text{vir}} \simeq 59\text{--}105$  kpc.

### 2.3. LAE Sample

The LAE sample is selected from the HETDEX survey and is described in LN22. It consists of 968 LAEs at  $1.9 < z < 3.5$  with narrow lines ( $\text{Ly}\alpha$  line FWHM  $< 1000$  km s<sup>-1</sup>) and  $\text{Ly}\alpha$  luminosities  $10^{42.4} \text{ erg s}^{-1} \lesssim L_{\text{Ly}\alpha} < 10^{43} \text{ erg s}^{-1}$ . These conditions remove most AGNs from the sample. Each LAE was observed once. Of these LAEs, 364 are at  $z < 2.35$ . The

equivalent widths of the Ly $\alpha$  and other lines measured from the median-stacked rest-frame spectrum are consistent with star formation being the main powering mechanism of the Ly $\alpha$  emission. To resolve Ly $\alpha$  halos, LN22 chose LAEs observed with PSF FWHM  $< 1''.4$  throughput  $> 0.13 = 40$ th percentile. While we do not know the SFR and stellar mass of this sample, LAEs at  $z \simeq 2.2$  with slightly lower Ly $\alpha$  luminosity ( $L_{\text{Ly}\alpha} \simeq 10^{42.3} \text{ erg s}^{-1}$ ) typically have SFR  $\simeq 14 M_{\odot} \text{ yr}^{-1}$  and stellar mass  $M_{\star} \simeq 5 \times 10^8 M_{\odot}$  (Nakajima et al. 2012). HET-DEX LAEs have similar SFR and stellar mass (McCarron et al. 2022).

### 3. Measurement of Ly $\alpha$ Halos

#### 3.1. Extraction of Surface Brightness and Stacking

We measure the Ly $\alpha$  halo profiles of the [O III] galaxies and around our comparative sample of LAEs following a similar procedure to LN22. The LAE profiles are consistent with each other. Because we do not detect individual Ly $\alpha$  emission lines of most [O III] galaxies, we assume that the observed Ly $\alpha$  line lies at the 3D-HST redshift. First, we remove continuum emission from the spectra to isolate Ly $\alpha$  from the continuum flux and to mitigate the impact of continuum emission from projected neighbors. From each fiber spectrum, we subtract the median flux between 11.7 and 40 Å (observed) away from the Ly $\alpha$  line on the red and blue sides. We then integrate the flux around the expected Ly $\alpha$  wavelength, obtaining an SB for each fiber. We choose an integration window of  $\lambda_{\text{Ly}\alpha}^{\text{obs}} \pm 10 \text{ Å}$  to account for the uncertainty of the expected observed Ly $\alpha$  wavelength due to the limited spectral resolution of the grism ( $R \simeq 130$ ).

The Ly $\alpha$  line can be redshifted by  $\simeq 200 \text{ km s}^{-1}$  from a galaxy's redshift because of radiative transfer effects (e.g., Nakajima et al. 2018). We tested redshifting the integration window by  $200 \text{ km s}^{-1}$  and subtracting the continuum on the red side of the shifted Ly $\alpha$  line. We also tested subtracting only the red continuum without shifting the line. Both tests produce a Ly $\alpha$  SB profile consistent with our results.

We define two LAE samples, the entire sample and the low-redshift ( $z < 2.35$ ) subsample. For the comparison with the entire LAE sample, we correct for cosmological SB dimming to the mean redshift (2.1) of the [O III] galaxy sample (factor  $(1+z)^4 \times (1+2.1)^{-4}$ ). For the comparison with previous results (Section 4.1), we convert the SB of each LAE and [O III] galaxy to surface luminosity to account for cosmological SB dimming. The surface luminosity  $\text{SL}_{\text{Ly}\alpha}$  relates to the surface brightness  $\text{SB}_{\text{Ly}\alpha}$  as  $\text{SL}_{\text{Ly}\alpha} = dL/dA_{\text{em}} = 4\pi (1+z)^4 \text{SB}_{\text{Ly}\alpha}$ , where  $dA_{\text{em}}$  is the surface area at emission.

We sort the fibers around each galaxy in each observation by their distance from the galaxy center and place them in radial bins with the bin edges at 5, 10, 15, 20, 30, 40, 60, 80, 160, 320, and 800 kpc.

We take the median of all fibers within each bin around each galaxy observation individually. Then we take the median of these radial profiles and estimate the uncertainty via a bootstrap algorithm. At least 355 (527) [O III] galaxies (galaxy observations) contribute to each bin.

#### 3.2. Estimating Systematic Uncertainty

We estimate the systematic uncertainty in two parts following the approach of LN22. The first estimates the background SB at the same wavelengths and in the same

observations as the galaxies separately for each galaxy sample. This background includes physical emission, e.g., from interlopers, sky emission residuals, and systematics introduced in the continuum subtraction. We calculate the median SB of all fibers farther away than 800 kpc from each galaxy observation. The median of these determines the background and a bootstrap algorithm determines the uncertainty. We find  $(1.51 \pm 0.02) \times 10^{-19} \text{ erg s}^{-1} \text{ cm}^{-2} \text{ arcsec}^{-2}$  for the [O III] galaxies. We subtract this background from the median profile of the galaxies.

The second part determines the systematic uncertainty of the median radial profile in the proximity of the galaxies. We repeat the stacking procedure 40 times, but with the central wavelength shifted between 20 and 210 Å in increments of 10 Å in both wavelength directions. Some galaxies at the blue end of the covered wavelength range have fewer than 40 wavelength-shifted profiles. The standard deviation per bin of these 40 Ly $\alpha$ -free profiles determines the systematic uncertainty of the median Ly $\alpha$  SB profile. The median ratio of this systematic uncertainty to the uncertainty from the bootstrap algorithm is 1.4. In each bin, we choose the larger of the two estimates as the final uncertainty. The mean and median of the wavelength-shifted profiles are consistent with the background SB.

We stack the radial profiles of stars from the Gaia DR 2 (Gaia Collaboration et al. 2018) in the same manner as Lujan Niemeyer et al. (2022) out to 100''. The median profile plateaus at  $10'' < r < 100''$ , presumably because of unmasked continuum sources and the lack of a continuum and background subtraction. We subtract the mean value at  $r > 10''$ . We obtain a separate star profile for the observations of LAEs and [O III] emitters and scale them to match the flux within 2'' of the galaxy profiles. Both profiles are modeled well by a Moffat function with  $\beta = 2.2$  with the mean seeing FWHM as the observations.

## 4. Results and Discussion

Figure 1 presents the median Ly $\alpha$  SB profile of the [O III] galaxies out to 800 kpc. The profile is significantly more extended than the star profile. Figure 1 also shows the median redshift-adjusted Ly $\alpha$  SB profile of the LAE sample at  $1.9 < z < 3.5$ . While the [O III]-galaxy profile is an order of magnitude fainter at  $r < 10 \text{ kpc}$ , it reaches a consistent SB at  $r > 40 \text{ kpc}$ . The profiles of the entire LAE sample and the subsample at  $z < 2.35$  are consistent at all radii.

Byrohl et al. (2021) find in their simulation that the photons in the core predominantly originate from the central galaxy, but those at large distances originate from other galaxies. Hence, the central SB should depend on the amount of photons escaping the central galaxy. At large distances, however, galaxies with similar CGM and clustering properties should have similar Ly $\alpha$  SB profiles.

While the intrinsic Ly $\alpha$  luminosities of the galaxy samples are unknown, the small Ly $\alpha$  escape fraction of the [O III] galaxies along the LOS can explain the lower surface brightness of the profile in the core. In contrast, Leclercq et al. (2017) find a weak positive correlation between the halo scale length and Ly $\alpha$  luminosity of the inner halo, implying that brighter LAEs have flatter halos. The similarity of the Ly $\alpha$  SB profiles of the two galaxy samples at  $r > 40 \text{ kpc}$  supports the picture in which the outer parts of the profiles are dominated by photons not related to Ly $\alpha$  emission produced

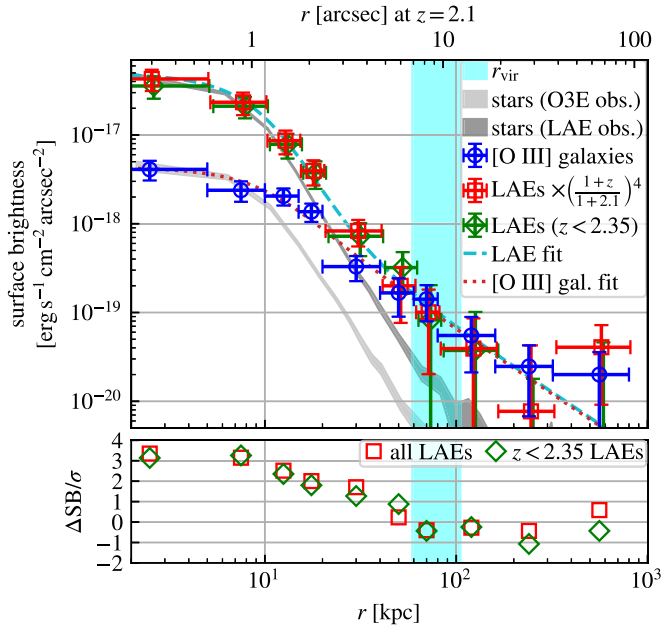


**Figure 1.** Top: median Ly $\alpha$  SB profile of 1034 [O III] galaxies (blue circles) compared to the redshift-adjusted profile of all LAEs (red squares) and the profile of the LAEs at  $z < 2.35$  (green diamonds). The LAE profiles are slightly shifted along the  $x$ -axis for better visibility. The star profile in the [O III] galaxy observations at  $z = 2.1$  and that in the LAE observations at  $z = 2.5$  are shown as light gray and dark gray areas, respectively. The cyan area shows the estimated virial radius of the host dark matter halos of the [O III] galaxies. The dotted and dashed lines show the best-fit PSF-plus-power-law model. Bottom: significance of the difference between the profiles, i.e., the difference between the [O III] profile and the LAE profiles divided by the uncertainties added in quadrature, with the same symbols as above.

in the central galaxy. The profiles are modeled well by a PSF-plus-power-law model, with power-law index  $-1.45$ , cut off at  $r_{\min} \simeq 2$  kpc. While the power-law component is designed to be identical, the best-fit PSF component of the LAE profile is 40 times brighter than that of the [O III] galaxies.

Figure 2 shows the median Ly $\alpha$  SB profiles of several subsamples of the [O III] galaxies. Most profiles are similar ( $< 2\sigma$  difference). The following differences are statistically significant ( $> 2\sigma$ ). The Ly $\alpha$  SB of the low- $L_{[\text{O III}]}$  sample is lower than that of the high- $L_{[\text{O III}]}$  sample at  $r < 60$  kpc. While the low- $L_{[\text{O III}]}$  profile follows the star profile out to 40 kpc, it increases to match the high- $L_{[\text{O III}]}$  profile at  $r > 60$  kpc. The subsamples with high dust attenuation, stellar mass, and SFR are fainter at  $r < 5$  kpc than those with low dust attenuation, stellar mass, and SFR, but similar at larger distances. This can be explained by lower escape fractions for those subsamples, consistent with the notion that the escape fraction anticorrelates with dust extinction, stellar mass, and SFR (Runnholm et al. 2020; Weiss et al. 2021). The profiles of the subsamples with low UV luminosity or below the SFR–stellar mass relation are similar to those with high UV luminosity or above the SFR–stellar mass relation at most radii, but fainter at intermediate distances, similar to the low- $L_{[\text{O III}]}$  subsample. This suggests that the SB is independent of the properties of the central galaxies at large distances. However, the uncertainties at large radii are large and more data are necessary for a clear conclusion. The similarity of the Ly $\alpha$  SB profiles at different stellar masses appears to contradict the result of Byrohl et al. (2021). Their fiducial model, which does not account for the destruction of Ly $\alpha$  photons by dust, indicates that the Ly $\alpha$  SB

is higher for galaxies with higher stellar mass out to large distances. When including dust treatment (see Appendix A4 of Byrohl et al. 2021), the correlation between stellar mass and outer Ly $\alpha$  SB level weakens because massive galaxies are more strongly affected by dust attenuation. The resulting Ly $\alpha$  SB profiles are more similar across stellar masses, better matching our findings.

#### 4.1. Comparison with Previous Results

Figure 3 compares the surface luminosity profile of [O III] galaxies and that of the LAEs with previous results for LAEs and LBGs at redshifts  $2 < z < 4$ . We show the profiles as a function of physical distance because most of the data lie within the virial radii of the galaxies. The profiles that were given as a function of comoving distance or did not contain the  $(1+z)^4$  factor were adjusted using one redshift for each sample (see caption of Figure 3). Because of the smaller PSF of MUSE, the profiles of Wisotzki et al. (2018) and Kusakabe et al. (2022) are steeper in the core than our profiles. We therefore show the convolved profiles with the PSF model following the stacked star profile in the [O III] galaxy observations (Moffat function with  $\beta = 2.2$  and FWHM = 1.47 convolved with the VIRUS fiber profile), as though VIRUS observed these profiles at  $z = 2.1$ . Despite differences at small distances, all LAE and LBG profiles are similar at intermediate distances ( $20 \text{ kpc} \lesssim r \lesssim 80 \text{ kpc}$ ).

#### 4.2. Emission Mechanism

##### 4.2.1. Star Formation in Other Galaxies

To find out whether the measured Ly $\alpha$  emission can be powered by star formation alone, we estimate the required star formation rate density (SFRD) from the measured Ly $\alpha$  luminosity within 800 kpc of the [O III] sample ( $L_{\text{Ly}\alpha} = (2.3 \pm 1.3) \times 10^{43} \text{ erg s}^{-1}$ ). Using  $L_{\text{Ly}\alpha} = 10^{42} \text{ erg s}^{-1} \times \text{SFR } M_{\odot}^{-1} \text{ yr}$  (see Dijkstra 2019), we find  $\text{SFRD} = 0.05 \pm 0.03 M_{\odot} \text{ yr}^{-1} \text{ cMpc}^{-3}$ . This value is smaller than that in the literature ( $\simeq 0.1 M_{\odot} \text{ yr}^{-1} \text{ cMpc}^{-3}$ ; summarized by Rowan-Robinson et al. 2016), implying that star-formation-induced photons can account for the Ly $\alpha$  emission out to 800 kpc.

##### 4.2.2. Star Formation in the Central Galaxy

The median SFR of the [O III] galaxies is  $10^{0.960} M_{\odot} \text{ yr}^{-1}$ . Using the same  $L_{\text{Ly}\alpha}$ –SFR relation as above, we expect an intrinsic Ly $\alpha$  luminosity  $L_{\text{Ly}\alpha}^{\text{int}} \simeq 9.1 \times 10^{42} \text{ erg s}^{-1}$ . Because this is consistent with the measured luminosity, the Ly $\alpha$  photons could originate from the central galaxies if the escape fraction is close to one. This scenario is disfavored because of the small measured escape fraction of  $6_{-0.5}^{+0.6}\%$  (Weiss et al. 2021), as well as the theoretically expected one. Using the standard relation for the optical depth due to dust extinction of Calzetti et al. (2000) and Verhamme et al. (2006) yields  $f_{\text{esc}}^{\text{Ly}\alpha} \leq \exp\{-\tau_{\text{dust}}^{\text{Ly}\alpha}\} \approx 0.21$  for the median  $E(B - V)$  of our sample.

##### 4.2.3. Fluorescence

Cantalupo et al. (2005) predict a Ly $\alpha$  SB through fluorescence from the UV background of  $3.67 \times 10^{-20} \text{ erg s}^{-1} \text{ cm}^{-2} \text{ arcsec}^{-2}$  at  $z \sim 3$ . The photoionization rate of the UV background changes little from  $z = 3$  to  $z = 2$  (Faucher-Giguère 2020). Accounting for cosmic dimming, this value would be  $\simeq 10^{-19} \text{ erg s}^{-1} \text{ cm}^{-2} \text{ arcsec}^{-2}$  at  $z = 2.1$ , which is consistent

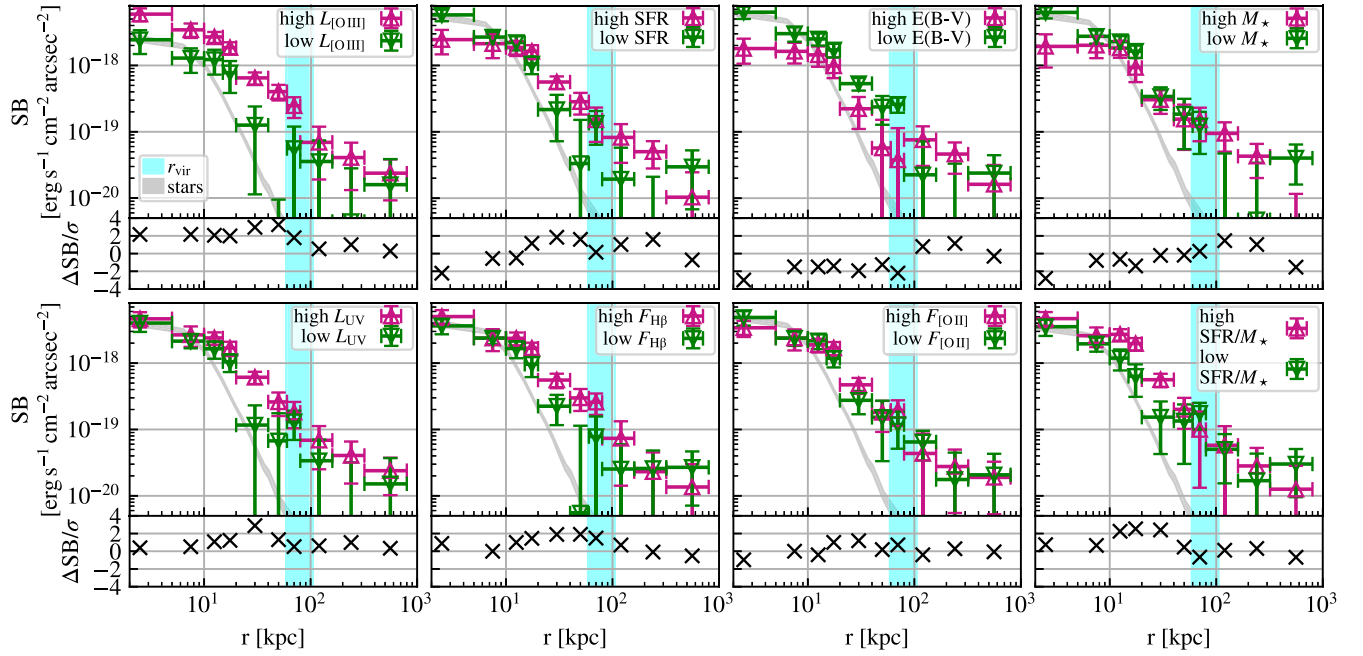


**Figure 2.** Median  $\text{Ly}\alpha$  SB profiles of differently separated subsamples. Except for the bottom right, each panel includes the subsample above (upward-facing magenta triangles) and below (downward-facing green triangles) the median of one property. The bottom-right panel shows the subsample above and below the linear  $\text{SFR}-M_*$  relation. The bottom part of each panel shows the significance of the difference between the two profiles.

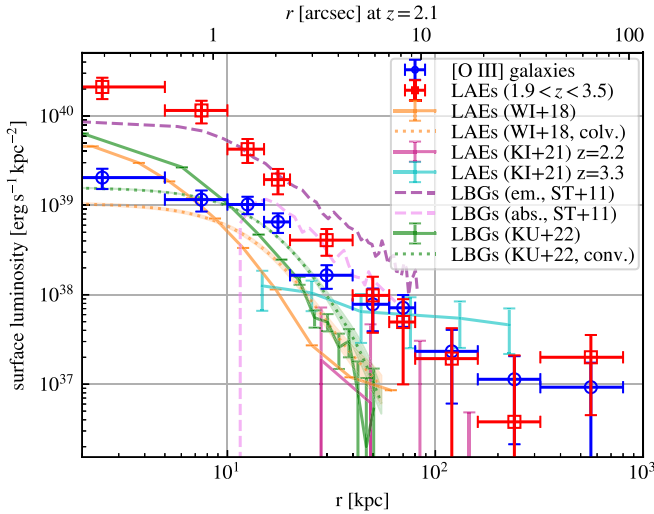


**Figure 3.** Comparison of the surface luminosity profile of the [O III] galaxies (blue circles) and that of the LAEs (red squares) with LAEs at  $z = 3-4$  (WI+18; Wisotzki et al. 2018), LAEs at  $z = 2.2$  and  $z = 3.3$  (KI+21; Kikuchi et al. 2022), LBGs with net  $\text{Ly}\alpha$  emission and absorption at  $z = 2.65$  (ST+11; Steidel et al. 2011), and LBGs at  $z = 3.56$  (KU+22; Kusakabe et al. 2022). The dotted profiles are convolved with the VIRUS PSF.

with the intermediate and outer points of the radial profiles, but too low to explain levels at small distances.

#### 4.2.4. Cooling Radiation

$\text{Ly}\alpha$  photons can be emitted through collisional excitation and recombination in cooling gas flowing into a galaxy. The subsequent scattering in an inflowing medium can lead to a blueshift of the  $\text{Ly}\alpha$  line (Dijkstra et al. 2006). While the scattering and blueshift may be negligible due to the low volume-filling factor of cold streams, we expect a filamentary morphology of the  $\text{Ly}\alpha$  emission (Dijkstra & Loeb 2009). We

cannot test whether the  $\text{Ly}\alpha$  line is blueshifted because of the low spectral resolution and the high redshift uncertainty of the [O III] galaxies. Detecting the filamentary structure requires deep observations of individual  $\text{Ly}\alpha$  halos rather than stacking and circular averaging.

## 5. Summary

We measure the  $\text{Ly}\alpha$  emission out to 800 kpc around 1034 [O III]-selected galaxies at  $1.9 < z < 2.35$ . While the central SB in the core ( $r < 10$  kpc) is fainter than that of the median redshift-adjusted  $\text{Ly}\alpha$  SB profile of 968 LAEs at  $1.9 < z < 3.5$  by an order of magnitude, the  $\text{Ly}\alpha$  SB in the outer parts ( $r > 40$  kpc) reaches the same surface brightness as that of the LAEs.

This result supports the picture in which photons originating from outside of the central galaxies dominate the  $\text{Ly}\alpha$  SB profiles at large radii. These photons either originate from other dark matter halos or satellite galaxies or are emitted through fluorescence or cooling radiation in the CGM. While we cannot exclude any of these sources, star formation alone can account for the integrated  $\text{Ly}\alpha$  emission out to 800 kpc, and fluorescence from the UV background is sufficient to explain the SB at intermediate distances.

We thank C. Byrohl for helpful and interesting discussions and F. Arrigoni Battaia, V. González Lobos, and C. Peroux for comments on the draft. We also thank the anonymous referee for the helpful review. E.K.'s work was supported in part by the Deutsche Forschungsgemeinschaft (DFG, German Research Foundation) under Germany's Excellence Strategy —EXC-2094-390783311.

HETDEX is led by the University of Texas at Austin, McDonald Observatory, and Department of Astronomy with participation from the Ludwig-Maximilians-Universität München, Max-Planck-Institut für Extraterrestrische Physik (MPE), Leibniz-Institut für Astrophysik Potsdam (AIP), Texas

A&M University, Pennsylvania State University, Institut für Astrophysik Göttingen, The University of Oxford, Max-Planck-Institut für Astrophysik (MPA), The University of Tokyo, and Missouri University of Science and Technology. In addition to Institutional support, HETDEX is funded by the National Science Foundation (grant AST-0926815), the State of Texas, the US Air Force (AFRL FA9451-04-2-0355), and generous support from private individuals and foundations.

The observations were obtained with the Hobby–Eberly Telescope (HET), which is a joint project of the University of Texas at Austin, the Pennsylvania State University, Ludwig-Maximilians-Universität München, and Georg-August-Universität Göttingen. The HET is named in honor of its principal benefactors, William P. Hobby and Robert E. Eberly.

VIRUS is a joint project of the University of Texas at Austin, Leibniz-Institut für Astrophysik Potsdam (AIP), Texas A&M University (TAMU), Max-Planck-Institut für Extraterrestrische Physik (MPE), Ludwig-Maximilians-Universität München, Pennsylvania State University, Institut für Astrophysik Göttingen, University of Oxford, Max-Planck-Institut für Astrophysik (MPA), and The University of Tokyo.

The authors acknowledge the Texas Advanced Computing Center (TACC) at The University of Texas at Austin for providing high-performance computing, visualization, and storage resources that have contributed to the research results reported in this paper (<http://www.tacc.utexas.edu>).













This work is based on observations taken by the 3D-HST Treasury Program (GO 12177 and 12328) with NASA/ESA HST, which is operated by the Association of Universities for Research in Astronomy, Inc., under NASA contract NAS5-26555.

The Institute for Gravitation and the Cosmos is supported by the Eberly College of Science and the Office of the Senior Vice President for Research at the Pennsylvania State University.

This research made use of NASA’s Astrophysics Data System Bibliographic Services.

*Software:* Astropy (Astropy Collaboration et al. 2018), Numpy (Harris et al. 2020), Scipy (Virtanen et al. 2020), Matplotlib (Hunter 2007).

#### ORCID iDs

Maja Lujan Niemeyer  <https://orcid.org/0000-0002-6907-8370>  
 William P. Bowman  <https://orcid.org/0000-0003-4381-5245>  
 Robin Ciardullo  <https://orcid.org/0000-0002-1328-0211>  
 Max Gronke  <https://orcid.org/0000-0003-2491-060X>  
 Eiichiro Komatsu  <https://orcid.org/0000-0002-0136-2404>  
 Maximilian Fabricius  <https://orcid.org/0000-0002-7025-6058>  
 Daniel J. Farrow  <https://orcid.org/0000-0003-2575-0652>  
 Steven L. Finkelstein  <https://orcid.org/0000-0001-8519-1130>  
 Karl Gebhardt  <https://orcid.org/0000-0002-8433-8185>  
 Caryl Gronwall  <https://orcid.org/0000-0001-6842-2371>  
 Gary J. Hill  <https://orcid.org/0000-0001-6717-7685>  
 Chenxu Liu  <https://orcid.org/0000-0001-5561-2010>

Erin Mentuch Cooper  <https://orcid.org/0000-0002-2307-0146>

Donald P. Schneider  <https://orcid.org/0000-0001-7240-7449>

Sarah Tuttle  <https://orcid.org/0000-0002-7327-565X>

Gregory R. Zeimann  <https://orcid.org/0000-0003-2307-0629>

#### References

- Astropy Collaboration, Price-Whelan, A. M., Sipőcz, B. M., et al. 2018, *AJ*, 156, 123
- Behroozi, P., Wechsler, R. H., Hearin, A. P., & Conroy, C. 2019, *MNRAS*, 488, 3143
- Bowman, W. P., Zeimann, G. R., Ciardullo, R., et al. 2019, *ApJ*, 875, 152
- Bowman, W. P., Zeimann, G. R., Nagaraj, G., et al. 2020, *ApJ*, 899, 7
- Bowman, W. P., Ciardullo, R., Zeimann, G. R., et al. 2021, *ApJ*, 920, 78
- Brammer, G. B., van Dokkum, P. G., Franx, M., et al. 2012, *ApJS*, 200, 13
- Bryan, G. L., & Norman, M. L. 1998, *ApJ*, 495, 80
- Byrohl, C., Nelson, D., Behrens, C., et al. 2021, *MNRAS*, 506, 5129
- Calzetti, D., Armus, L., Bohlin, R. C., et al. 2000, *ApJ*, 533, 682
- Cantalupo, S., Porciani, C., Lilly, S. J., & Miniati, F. 2005, *ApJ*, 628, 61
- Dijkstra, M. 2019, Lyman-alpha as an Astrophysical and Cosmological Tool, Saas-Fee Advanced Course, Vol. 46 (Berlin: Springer), doi:10.1007/978-3-662-59623-4\_1
- Dijkstra, M., Haiman, Z., & Spaans, M. 2006, *ApJ*, 649, 14
- Dijkstra, M., & Loeb, A. 2009, *MNRAS*, 400, 1109
- Erb, D. K., Pettini, M., Steidel, C. C., et al. 2016, *ApJ*, 830, 52
- Faucher-Giguère, C-A 2020, *MNRAS*, 493, 1614
- Gaia Collaboration, Brown, A. G. A., Vallenari, A., et al. 2018, *A&A*, 616, A1
- Gebhardt, K., Mentuch Cooper, E., Ciardullo, R., et al. 2021, *ApJ*, 923, 217
- Gould, A., & Weinberg, D. H. 1996, *ApJ*, 468, 462
- Grogin, N. A., Kocevski, D. D., Faber, S. M., et al. 2011, *ApJS*, 197, 35
- Hagen, A., Zeimann, G. R., Behrens, C., et al. 2016, *ApJ*, 817, 79
- Haiman, Z., Spaans, M., & Quataert, E. 2000, *ApJL*, 537, L5
- Harris, C. R., Millman, K. J., van der Walt, S. J., et al. 2020, *Natur*, 585, 357
- Hathi, N. P., Le Fèvre, O., Ilbert, O., et al. 2016, *A&A*, 588, A26
- Hill, G. J., Lee, H., MacQueen, P. J., et al. 2021, *AJ*, 162, 298
- Hunter, J. D. 2007, *CSE*, 9, 90
- Kikuchihara, S., Harikane, Y., Ouchi, M., et al. 2022, *ApJ*, 931, 97
- Koekemoer, A. M., Faber, S. M., Ferguson, H. C., et al. 2011, *ApJS*, 197, 36
- Kusakabe, H., Verhamme, A., Blaizot, J., et al. 2022, *A&A*, 660, A44
- Leclercq, F., Bacon, R., Wisotzki, L., et al. 2017, *A&A*, 608, A8
- Lujan Niemeyer, M., Komatsu, E., Byrohl, C., et al. 2022, *ApJ*, 929, 90
- Mas-Ribas, L., Dijkstra, M., Hennawi, J. F., et al. 2017, *ApJ*, 841, 19
- McCarron, A. 2022, *ApJ*, submitted
- Momcheva, I. G., Brammer, G. B., van Dokkum, P. G., et al. 2016, *ApJS*, 225, 27
- Nakajima, K., Fletcher, T., Ellis, R. S., Robertson, B. E., & Iwata, I. 2018, *MNRAS*, 477, 2098
- Nakajima, K., Ouchi, M., Shimasaku, K., et al. 2012, *ApJ*, 745, 12
- Ouchi, M. 2019, Lyman-alpha as an Astrophysical and Cosmological Tool: Saas-Fee Advanced Course, Vol. 46 (Berlin: Springer), doi:10.1007/978-3-662-59623-4\_3
- Planck Collaboration, Aghanim, N., Akrami, Y., et al. 2020, *A&A*, 641, A6
- Reddy, N. A., Topping, M. W., Shapley, A. E., et al. 2022, *ApJ*, 926, 31
- Rowan-Robinson, M., Oliver, S., Wang, L., et al. 2016, *MNRAS*, 461, 1100
- Runholm, A., Hayes, M., Melinder, J., et al. 2020, *ApJ*, 892, 48
- Shimakawa, R., Kodama, T., Shibuya, T., et al. 2017, *MNRAS*, 468, 1123
- Steidel, C. C., Bogosavljević, M., Shapley, A. E., et al. 2011, *ApJ*, 736, 160
- Trainor, R. F., Strom, A. L., Steidel, C. C., & Rudie, G. C. 2016, *ApJ*, 832, 171
- Trainor, R. F., Strom, A. L., Steidel, C. C., et al. 2019, *ApJ*, 887, 85
- Verhamme, A., Schaerer, D., & Maselli, A. 2006, *A&A*, 460, 397
- Virtanen, P., Gommers, R., Oliphant, T. E., et al. 2020, *Nat. Methods*, 17, 261
- Weiss, L. H., Bowman, W. P., Ciardullo, R., et al. 2021, *ApJ*, 912, 100
- Wisotzki, L., Bacon, R., Blaizot, J., et al. 2016, *A&A*, 587, A98
- Wisotzki, L., Bacon, R., Brinchmann, J., et al. 2018, *Natur*, 562, 229